Electronic Supplementary Information:

Gentle tension stabilizes atomically thin metallenes

Kameyab Raza Abidi and Pekka Koskinen*
Nanoscience Center, Department of Physics, University of Jyväskylä, 40014 Jyväskylä, Finland

Computational methods

The first-principles calculations were conducted using spin-polarized density-functional theory (DFT), as incorporated in the QuantumATK (U-2022.12) package [1]. The electronic interactions were modeled through the generalized gradient approximation with the Perdew-Burke-Ernzerhof (GGA-PBE) exchange-correlation functional [2]. Core electron effects were treated using high-quality PseudoDojo pseudopotentials [3], and the valence electron wavefunctions were expanded using an LCAO-*medium* basis set, a level of theory previously validated for capturing essential features of low-dimensional metallic bonding and well sufficient for our purposes of investigating stability trends [4].

The Brillouin zones for all 2D lattices were sampled by the Monkhorst-Pack $13 \times 13 \times 1$ k-point mesh [5]. A vacuum region of 10 Å was introduced in the non-periodic directions to decouple the lattices from spurious interactions across periodic images. Geometry optimization was done by the LBFGS algorithm for $<10^{-4}\,\mathrm{eV\,Å^{-1}}$ residual forces [6], together with a total energy convergence criterion of $10^{-8}\,\mathrm{eV}$. The buckled lattices with $t = 0$ are practically the same as corresponding flat lattices. All systems were modeled using computational unit cells similar to those in a previous work [7].

We calculated phonon dispersion across the entire Brillouin zone using the supercell approach to probe the dynamical stability. Specifically, we used $5 \times 5 \times 1$ supercells for square and honeycomb lattices and $5 \times 3 \times 1$ supercells for hexagonal lattices. Owing to the inherent numerical sensitivity of phonon calculations [8, 9], we imposed a more stringent force convergence criterion of $10^{-6}\,\mathrm{eV\,Å^{-1}}$ paired with a 20-Å vacuum.

For the molecular dynamics (MD) simulations, we used the Langevin thermostat as proposed by Goga *et al.* [10]. The thermostat was modeled with a 5-fs time step and $2 \times 10^{-4}\,\mathrm{fs^{-1}}$ friction coefficient. The MD simulation for the 2018-atom system with coexisting buckled honeycomb and flat hexagonal lattices (Fig. 4b) was performed by using the embedded atom method potential [11]. The potential reproduces the essential trends in the cohesion energy

* pekka.j.koskinen@jyu.fi

compared to DFT simulations (Au and Au Force Field in Fig. S1). Quantitative differences exist, but both methods yield a dynamically stable buckled honeycomb lattice at $a \lesssim 4$ Å^2 and a dynamically stable flat hexagonal lattice at $a \gtrsim 6$ Å^2 with equal slopes. Consequently, using a larger system and longer time scale, the more efficient force field could be used to conduct a proof-of-principle MD simulation of phase coexistence. The duration of the full MD simulation was 0.25 ns.

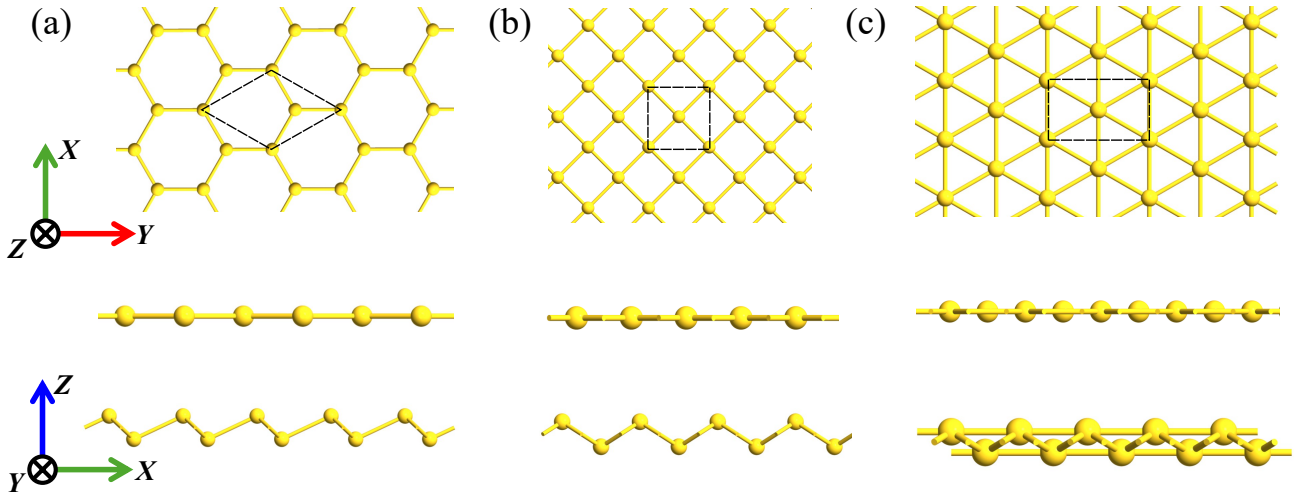

Fig. S1. Schematic views of (a) honeycomb, (b) square, and (c) hexagonal lattices with top views (top), side views of flat lattices (middle), and side views of buckled lattices (bottom). The dashed black lines represent the simulation cells. The thicknesses, bond lengths, and specific areas are coupled by the relations $d = \sqrt{\frac{4a}{3\sqrt{3}} + t^2}$ (honeycomb), $d = \sqrt{a + t^2}$ (square), and $d = \sqrt{\frac{2a}{\sqrt{3}} + t^2}$ (hexagonal), with $t = 0$ for flat lattices.

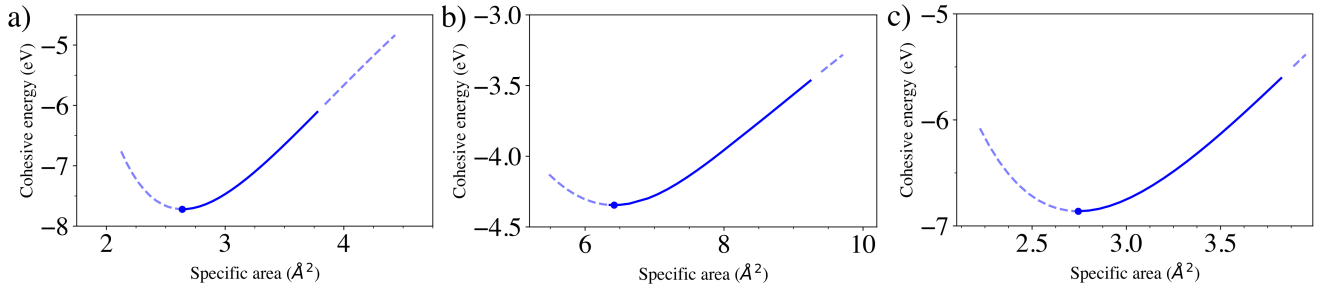

Fig. S2. The dependence of 2D dynamical stability on atom density for a) graphene, b) silicene, and c) hexagonal boron nitride (hBN).

Fig. S4 (on pages below). The figures show the dependence of 2D dynamical stability on atom density for 45 elements. a) The cohesive energies of the six lattices (dashed lines) and the dynamically stable intervals (solid segments). The energy scale is from gas phase atoms (zero) to 3D bulk cohesion (minimum). Dots denote the energy minima. Insets: the thickness of buckled lattices as a function of atom density. b) Phonon dispersion spectra of Au at different densities. Dynamically stable configurations (solid lines; middle of stable segments) have phonon modes with positive energies, whereas dynamically unstable ones (dashed lines; energy minima or the nearest unstable configuration at a smaller density) also have phonon modes with negative energies, implying imaginary frequencies and saddle points in the potential energy surface. The results for Au are shown using both DFT and force field.

Group 1

Li)

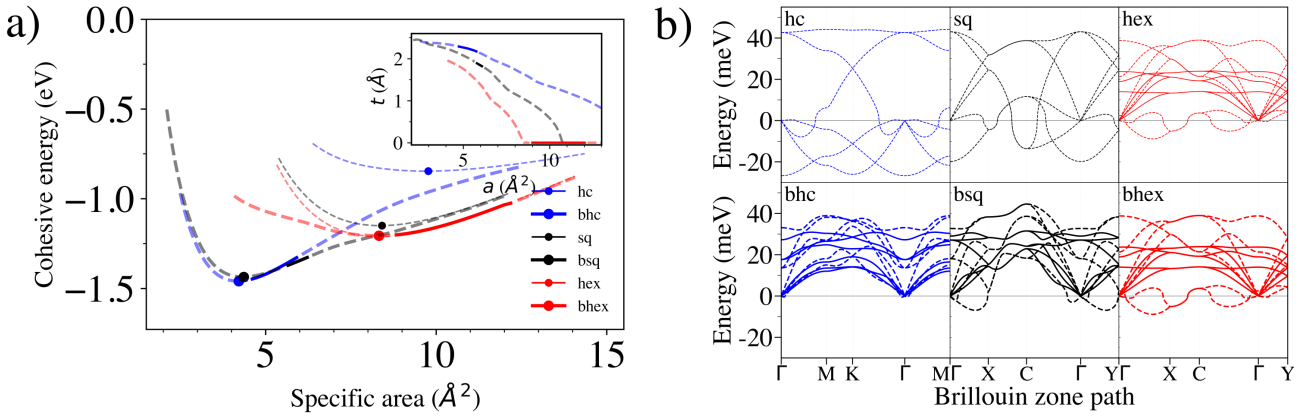

Na)

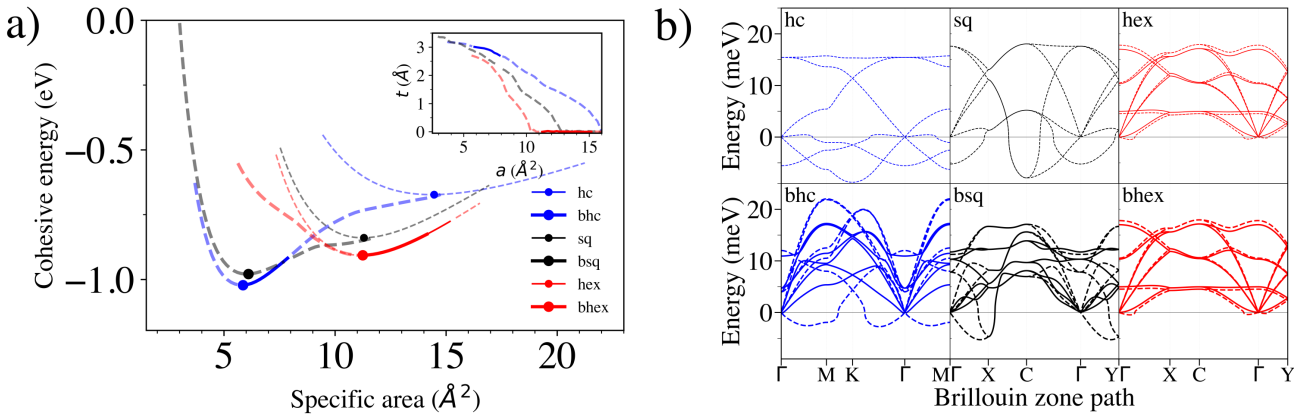

K)

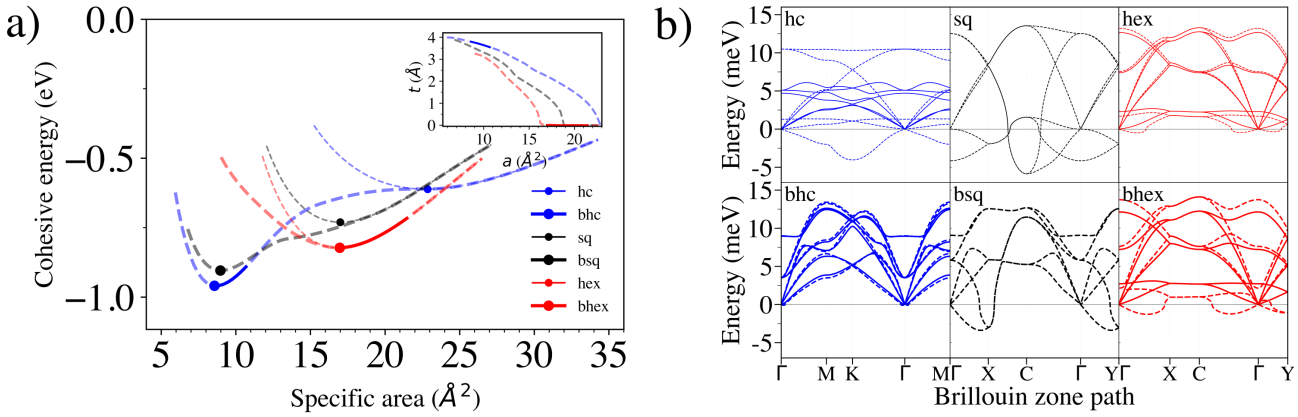

Rb)

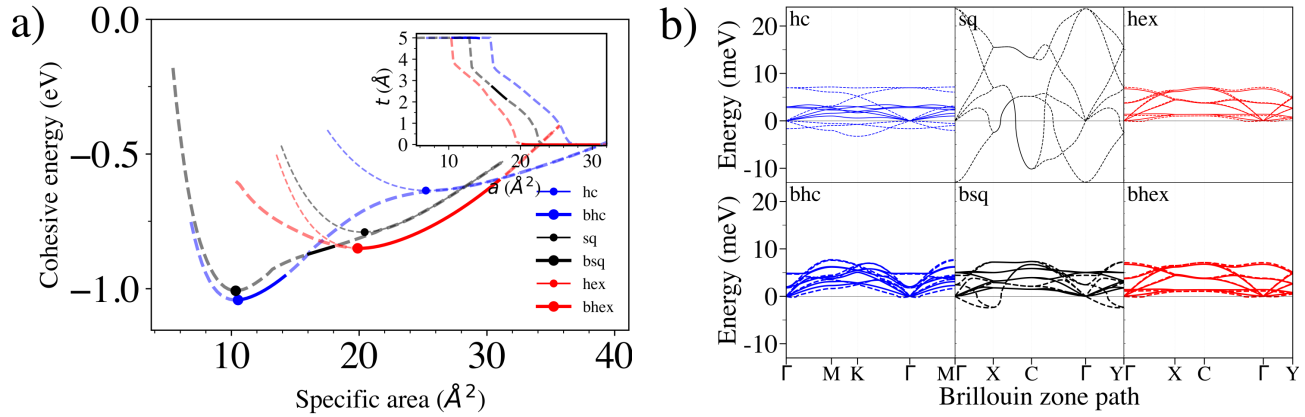

Cs)

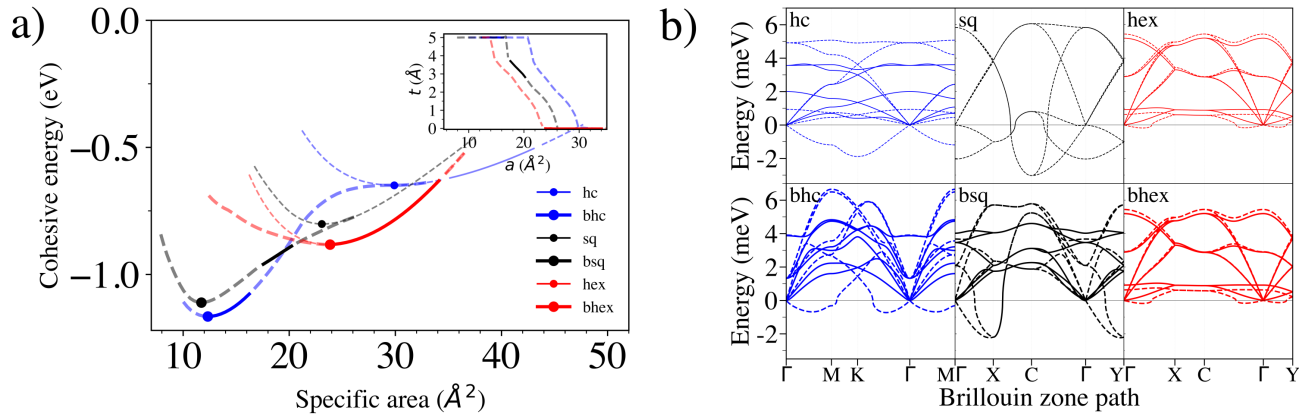

Group 2

Be)

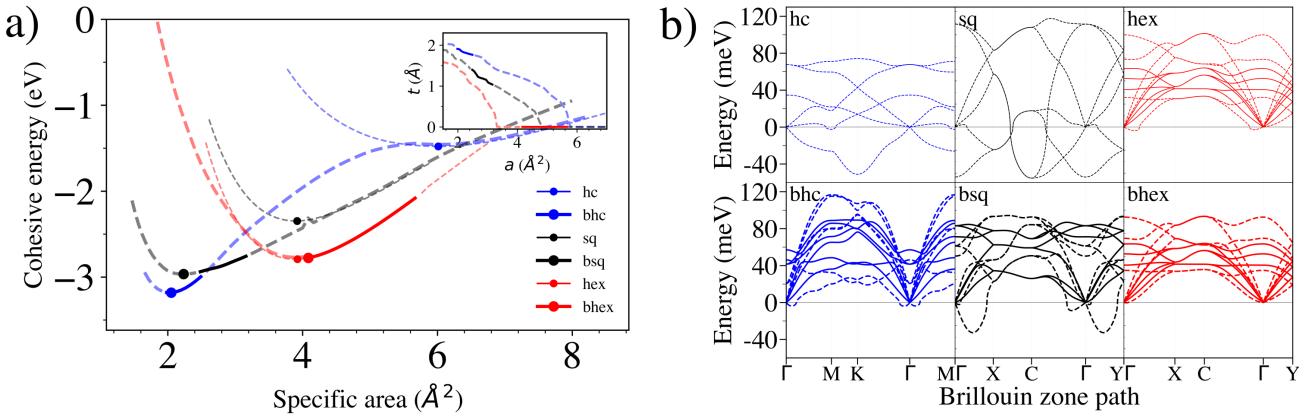

Mg)

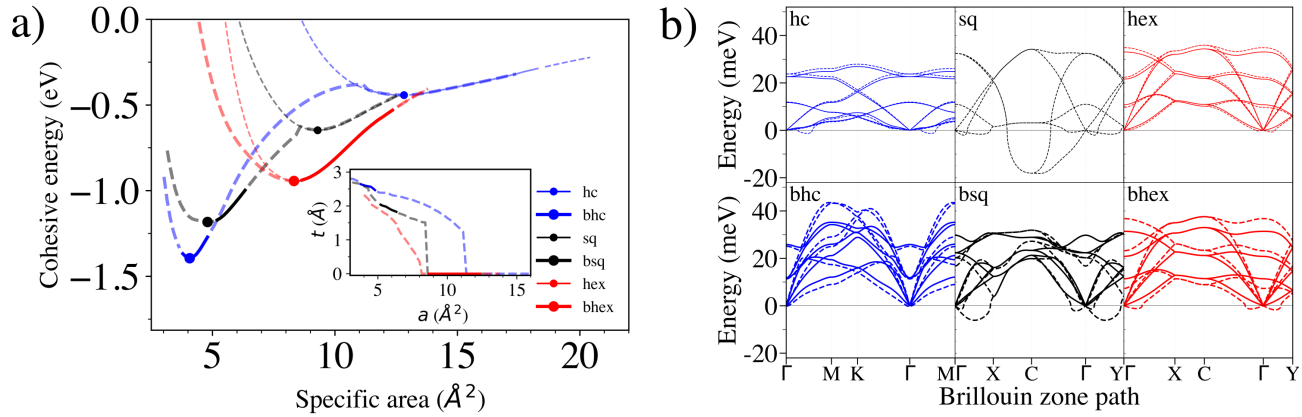
a)
Cohesive energy (eV)
Specific area (Å²)
t (Å)
a (Å²)
hc
bhc
sq
bsq
hex
bhex
b)
Energy (meV)
hc
sq
hex
bhc
bsq
bhex
Γ M K Γ M Γ X C Γ Y Γ X C Γ Y
Brillouin zone path

Ca)

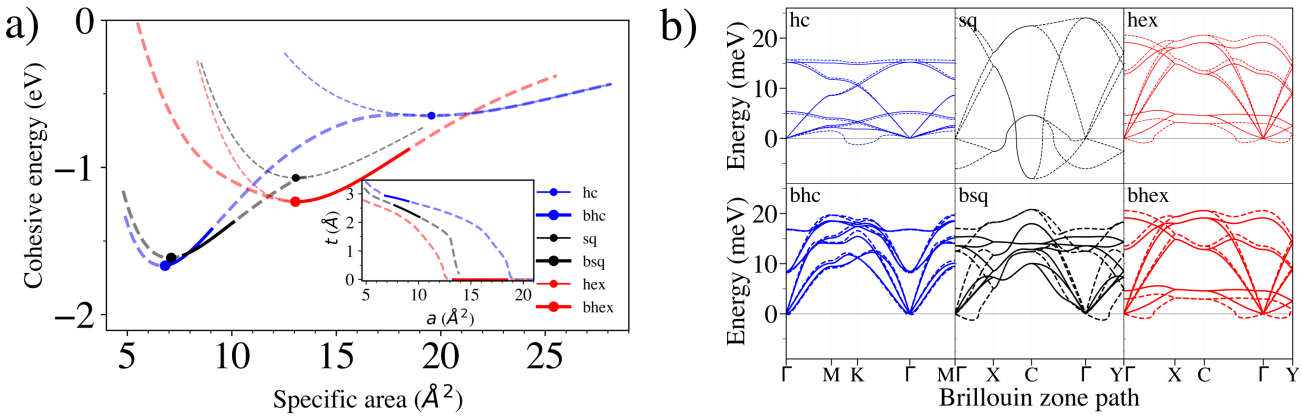
a)
Cohesive energy (eV)
Specific area (Å²)
t (Å)
a (Å²)
hc
bhc
sq
bsq
hex
bhex
b)
Energy (meV)
hc
sq
hex
bhc
bsq
bhex
Γ M K Γ M Γ X C Γ Y Γ X C Γ Y
Brillouin zone path

Sr)

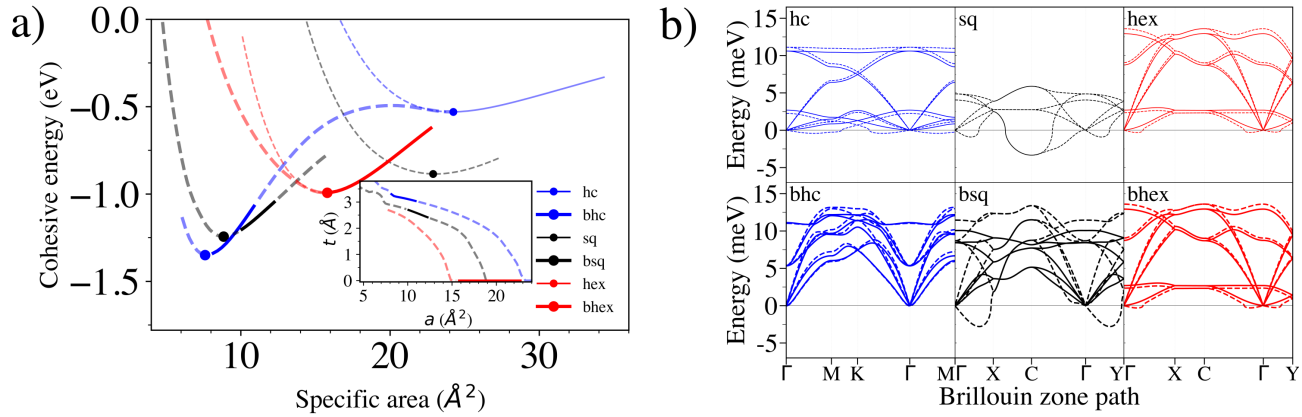
a)
Cohesive energy (eV)
Specific area (Å²)
t (Å)
a (Å²)
hc
bhc
sq
bsq
hex
bhex
b)
Energy (meV)
hc
sq
hex
bhc
bsq
bhex
Γ M K Γ M Γ X C Γ Y Γ X C Γ Y
Brillouin zone path

Ba)

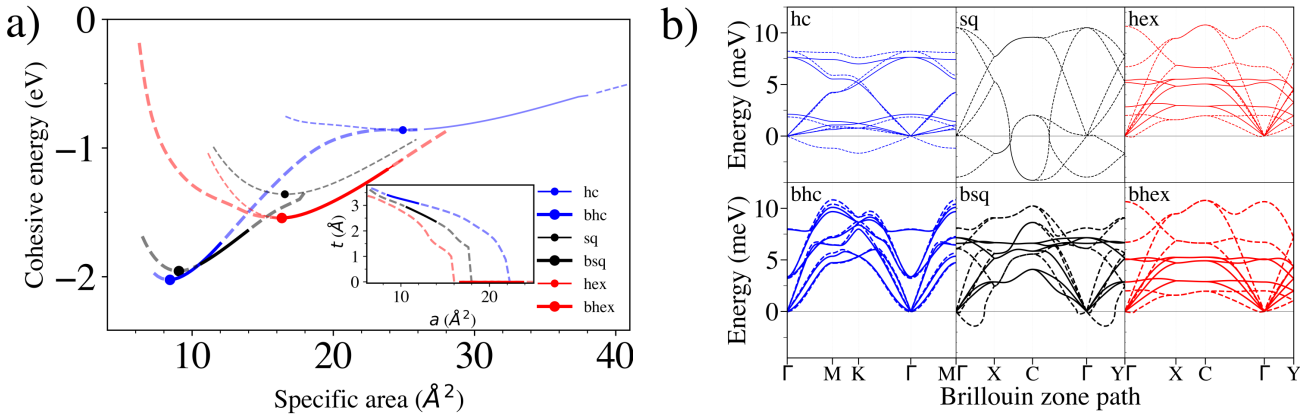

Group 3

Sc)

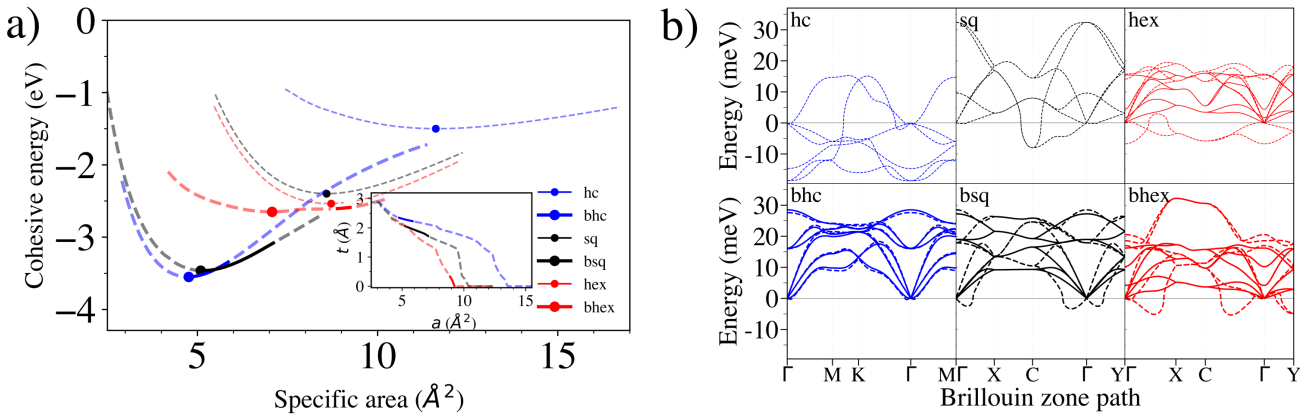

Y)

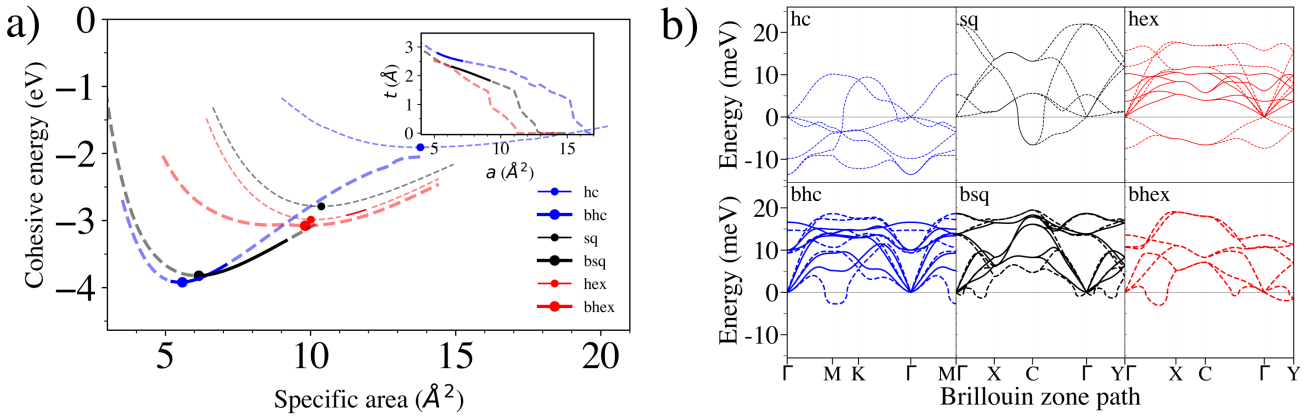

Group 4

Ti)

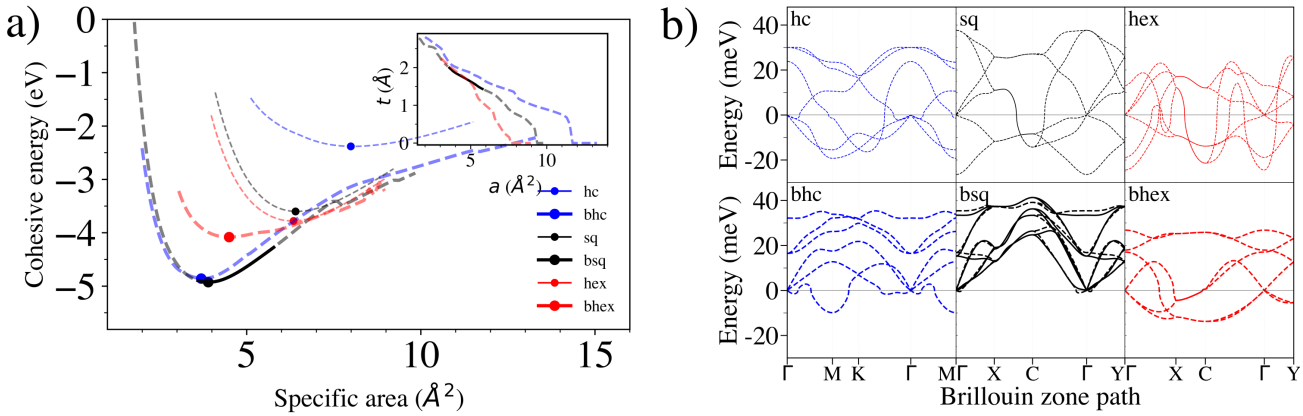

Zr)

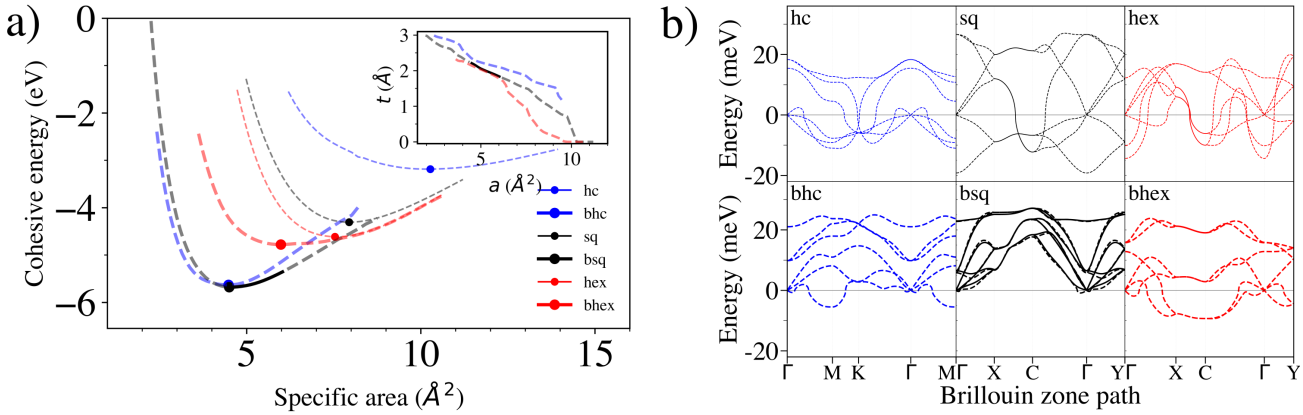

Hf)

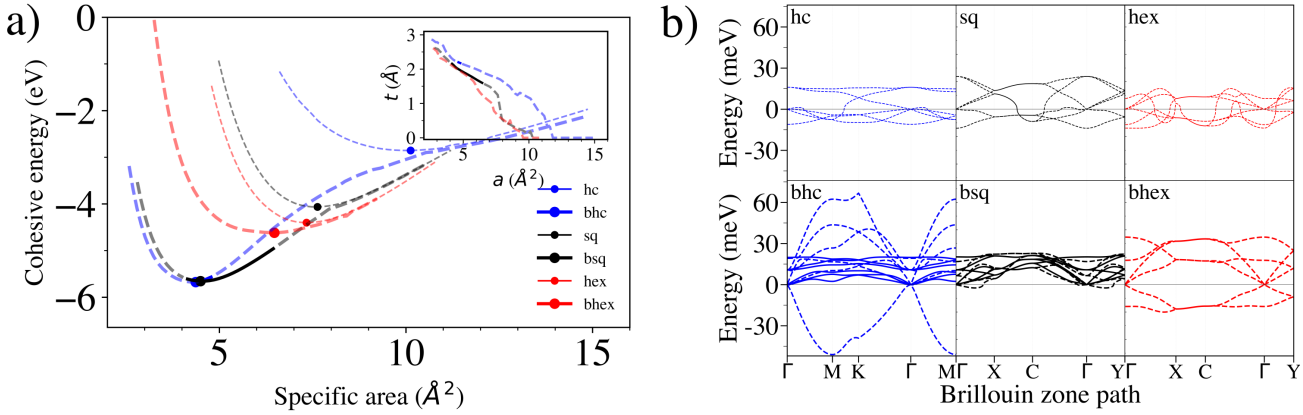

Group 5

V)

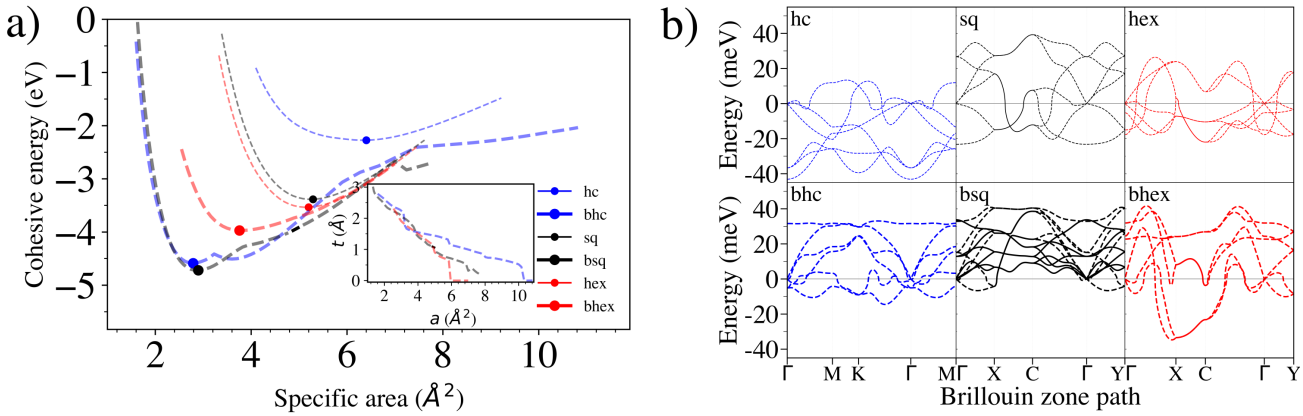

Nb)

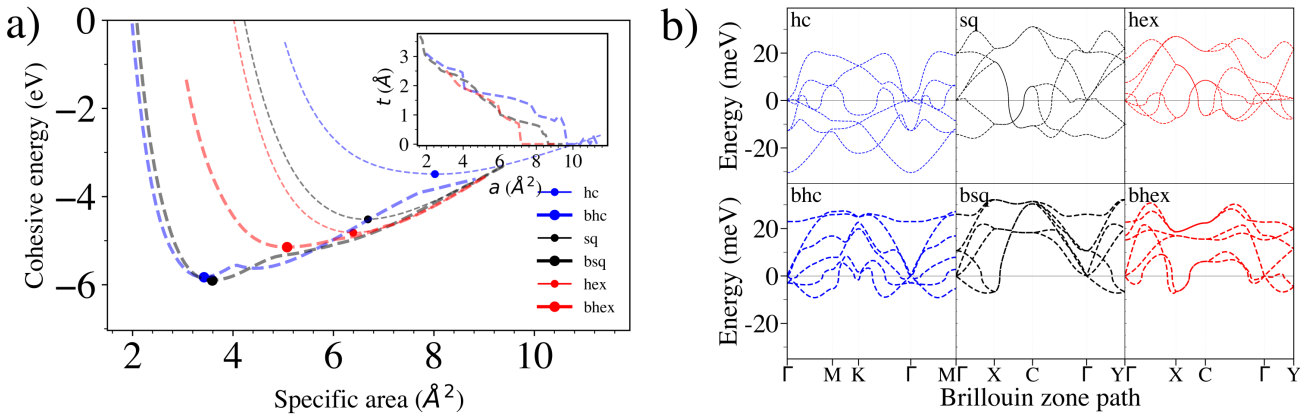

Ta)

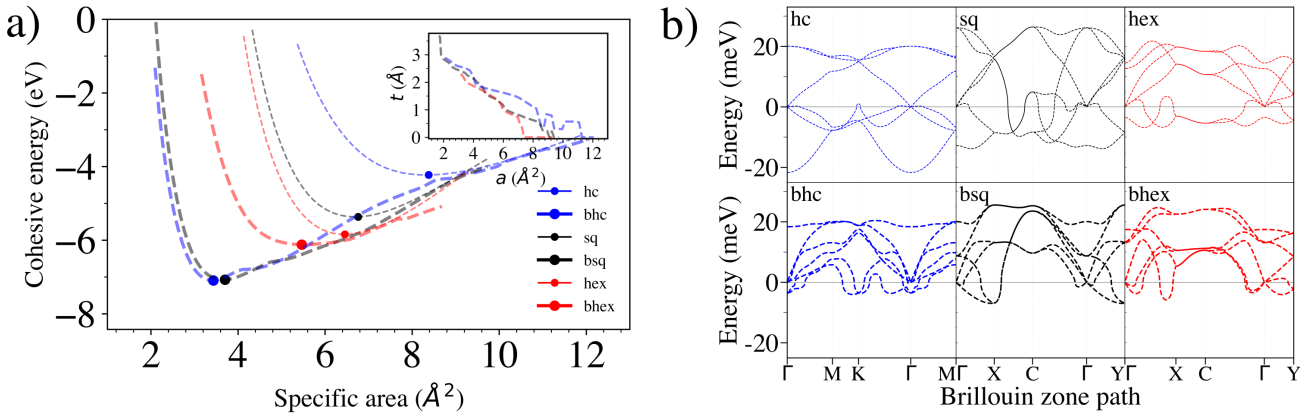

Group 6

Cr)

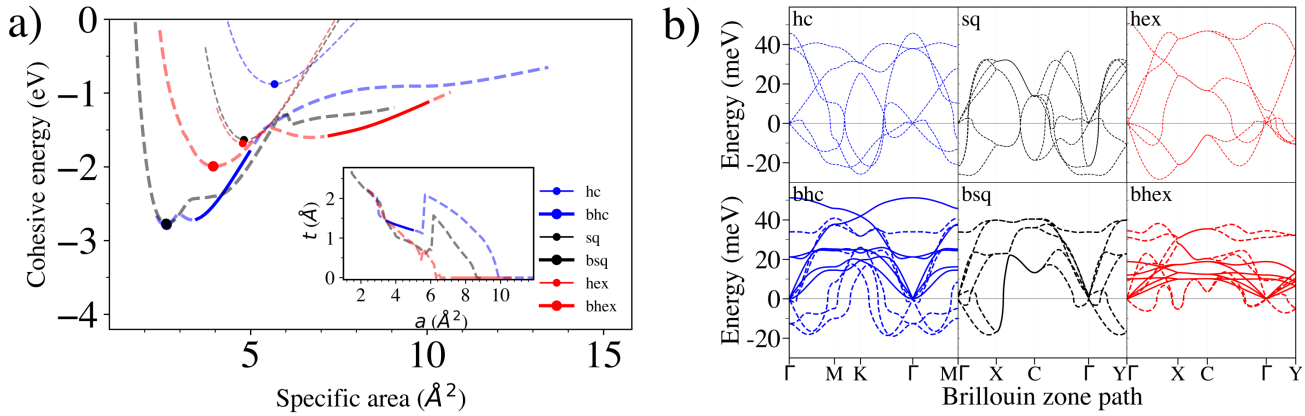

Mo)

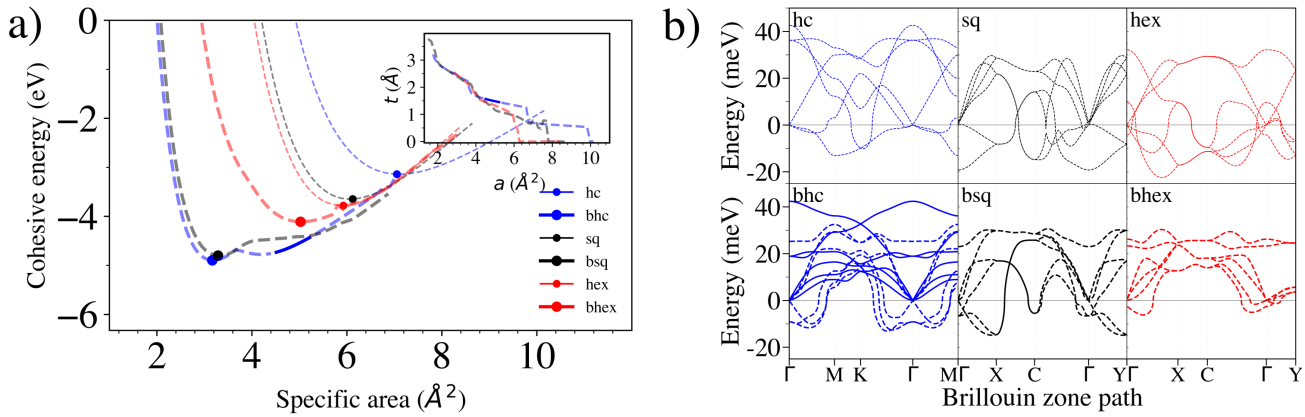

W)

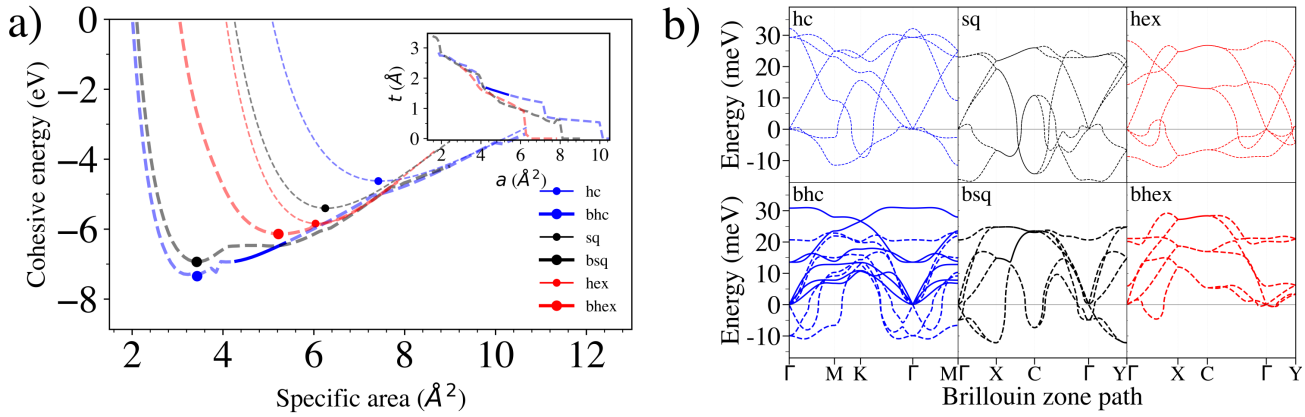

Group 7

Mn)

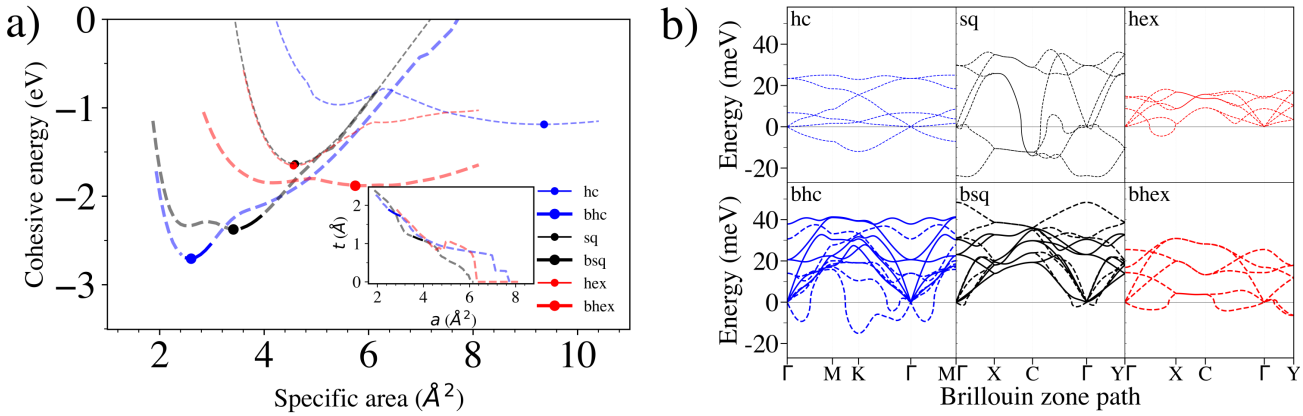

Re)

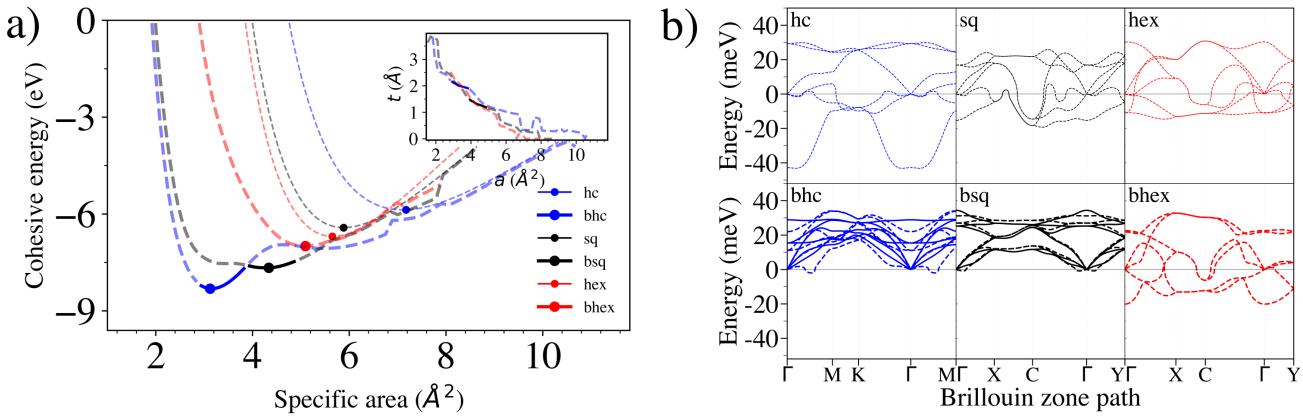

Group 8

Fe)

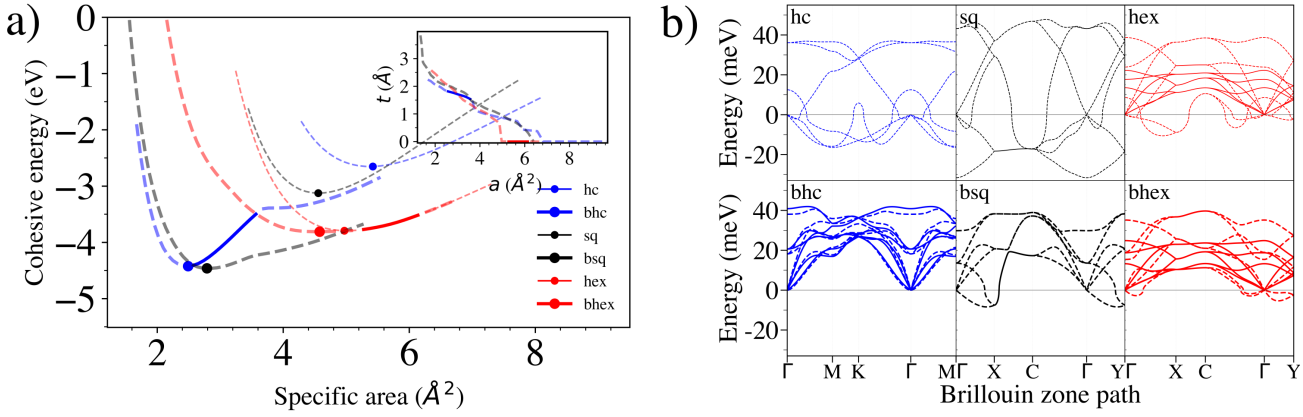

Ru)

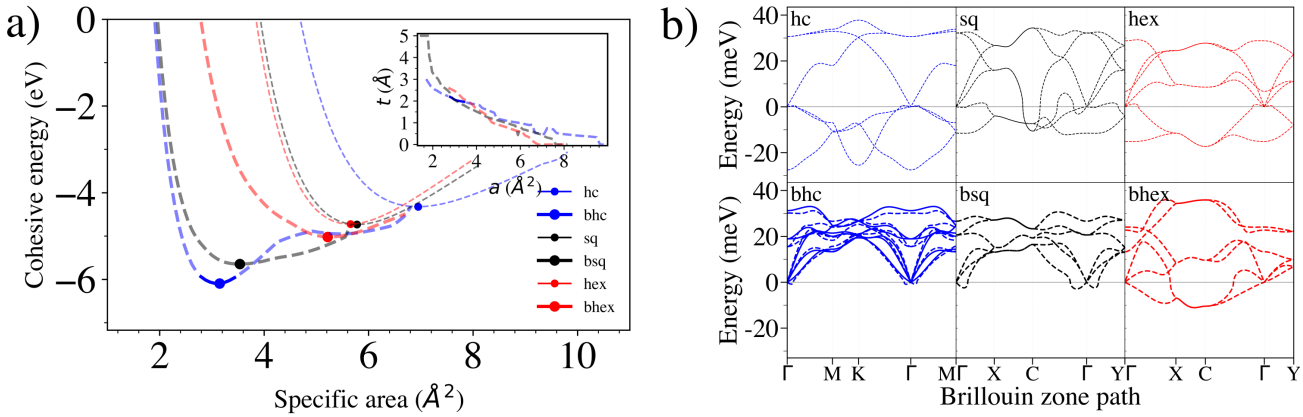

Os)

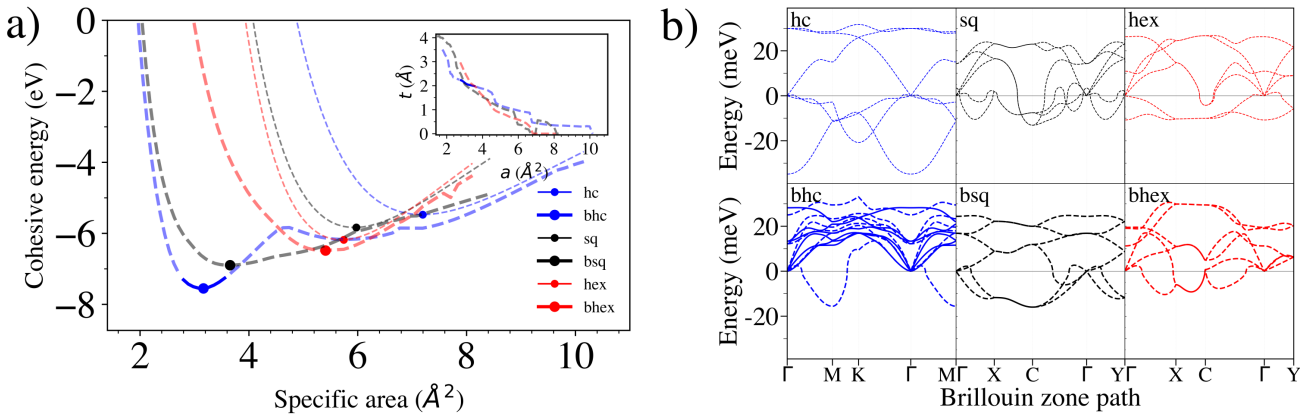

Group 9

Co)

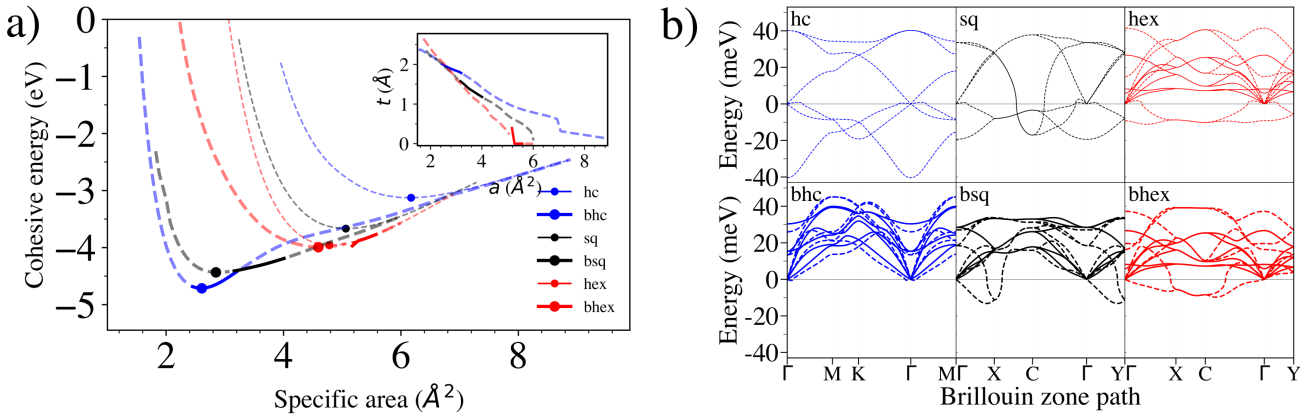

Rh)

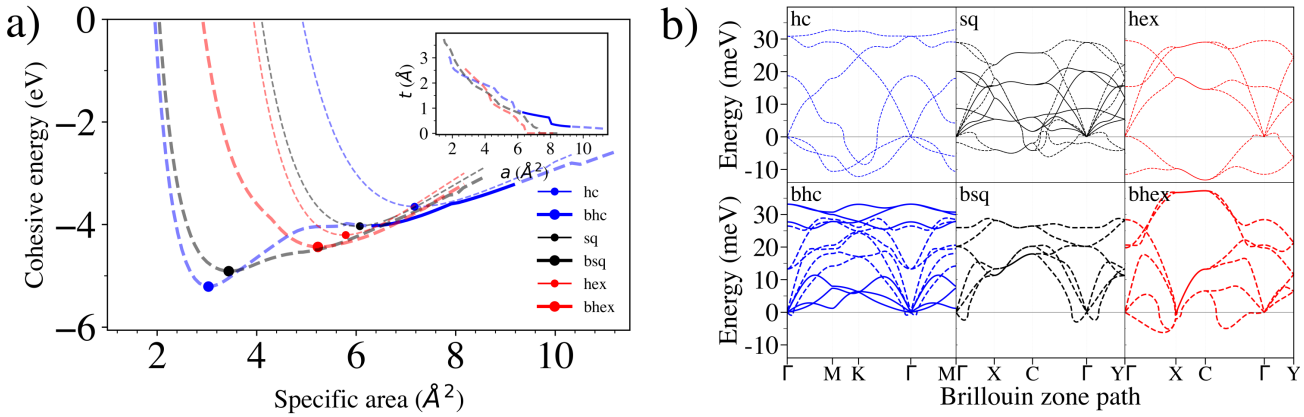

Ir)

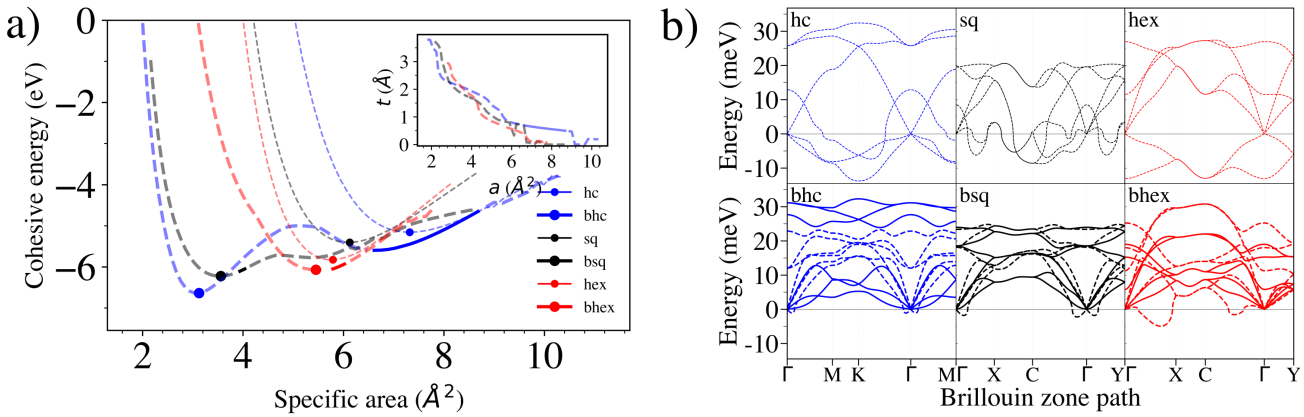

Group 10

Ni)

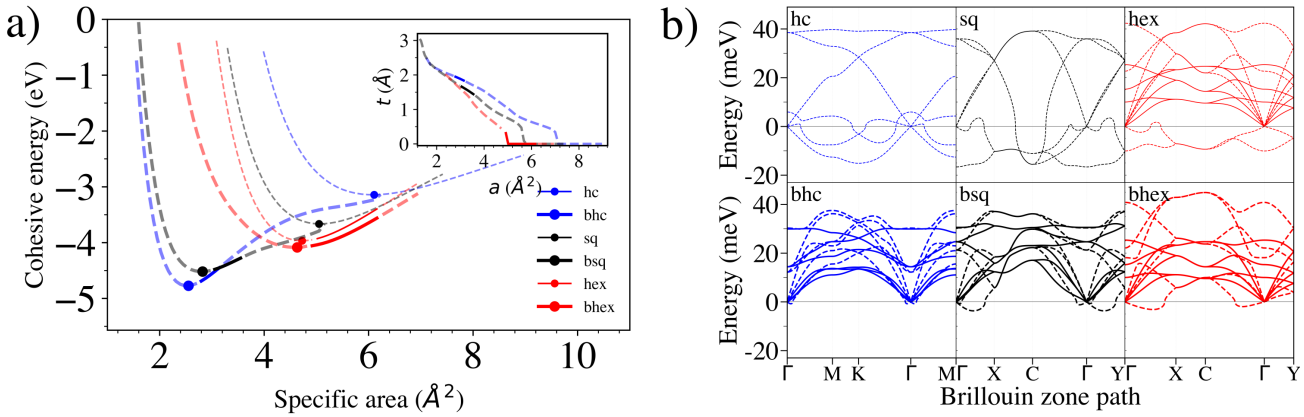

Pd)

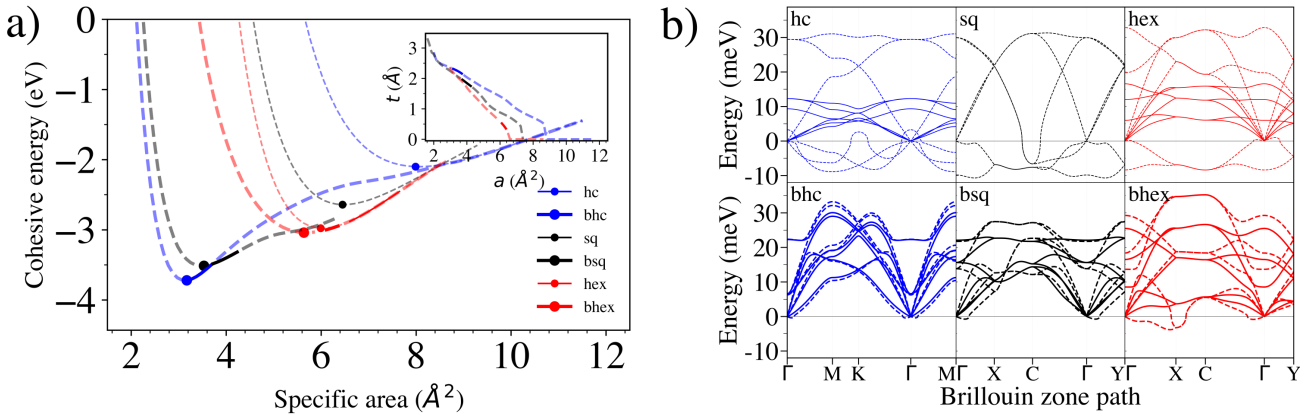

Pt)

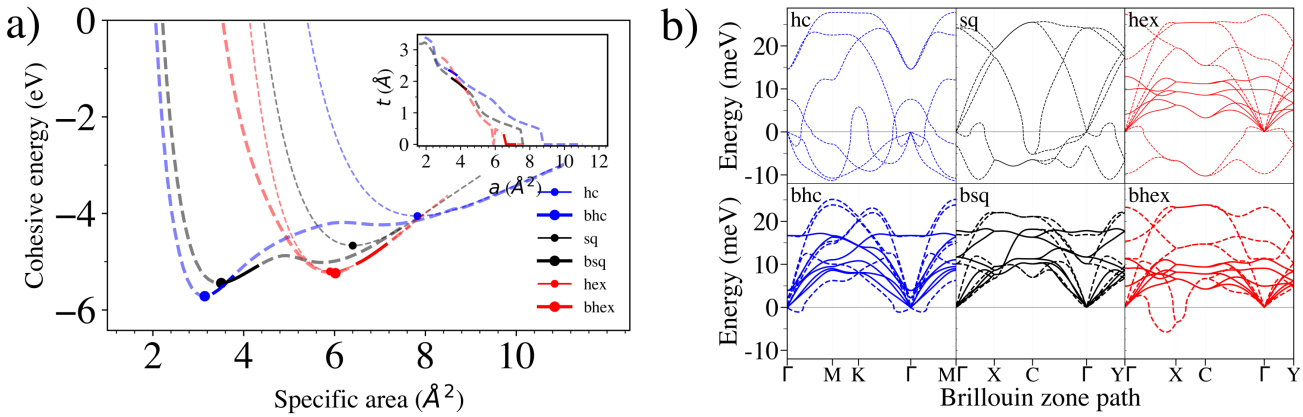

Group 11

Cu)

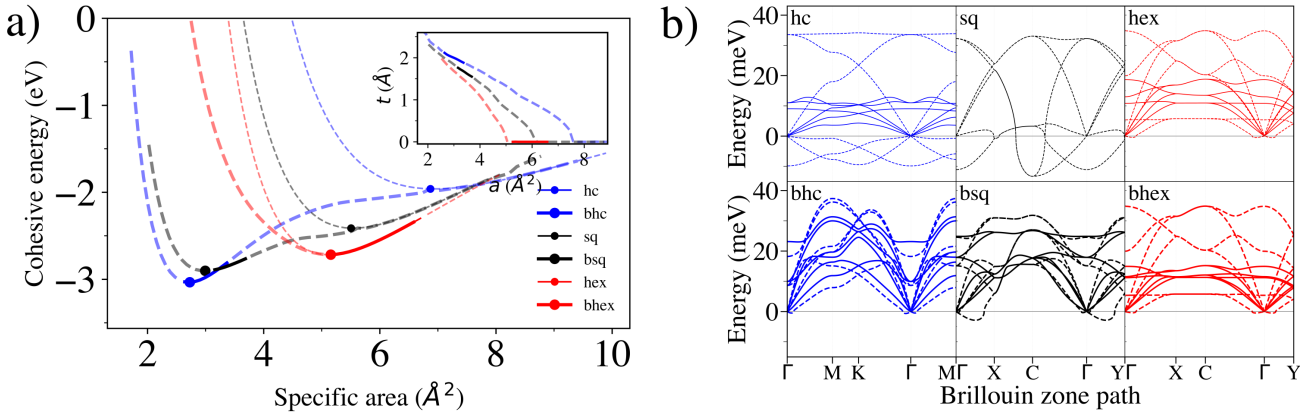

Ag)

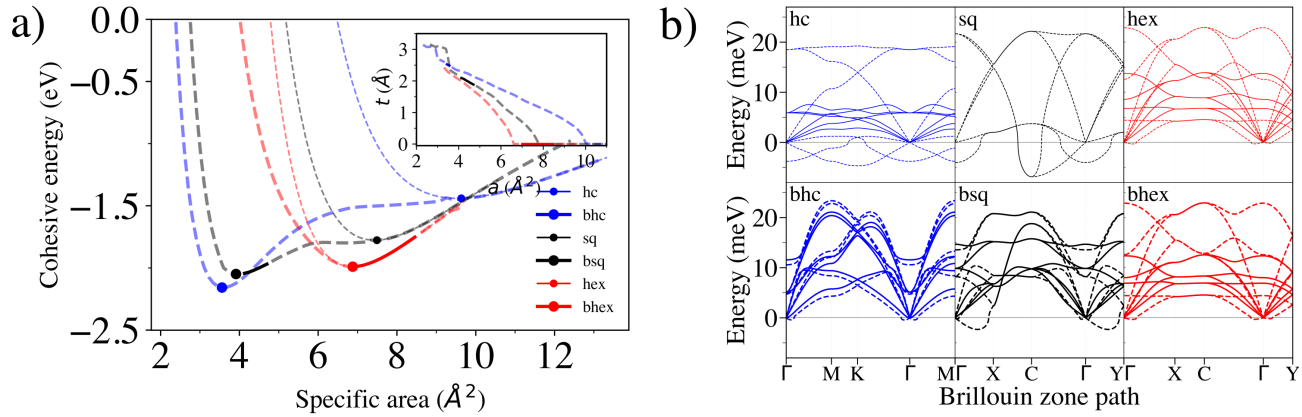

Au)

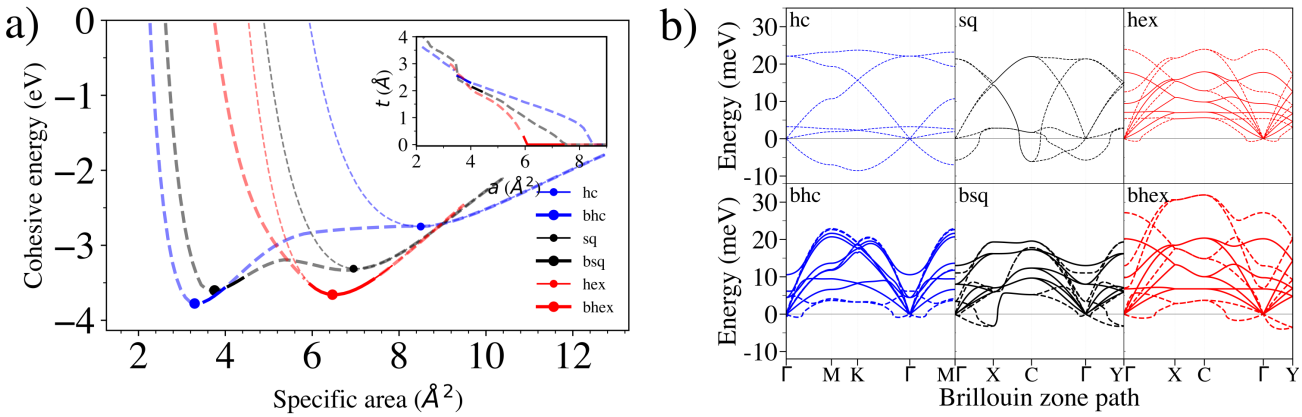

Au Force Field)

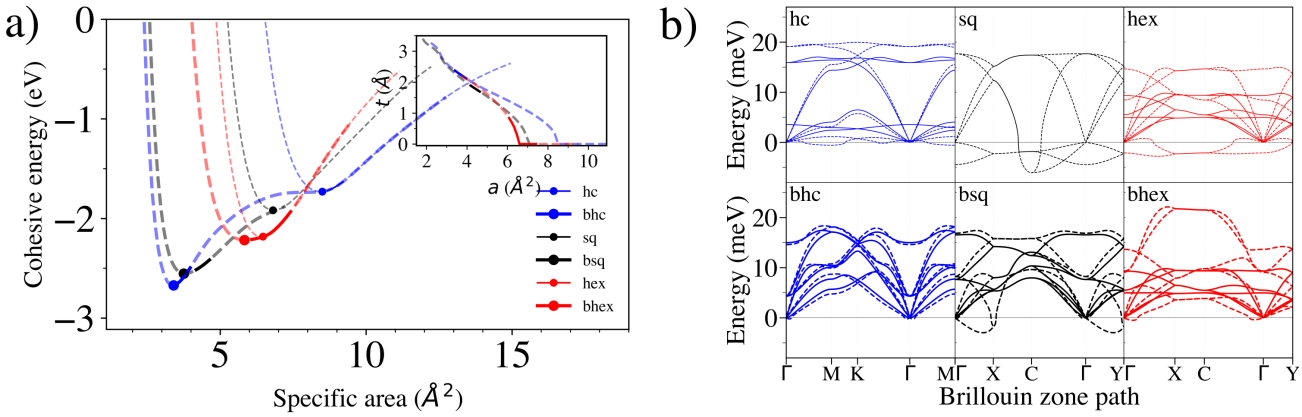

Group 12

Zn)

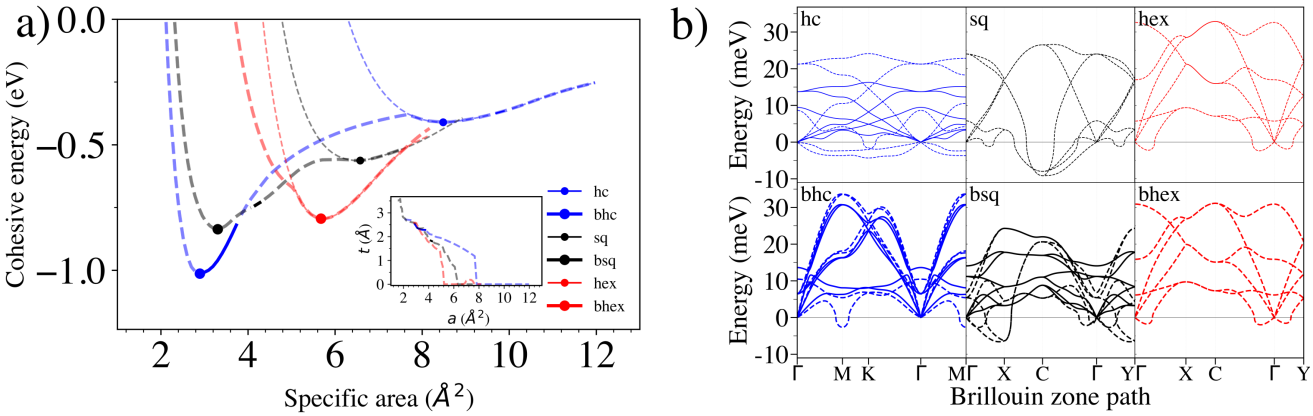

Cd)

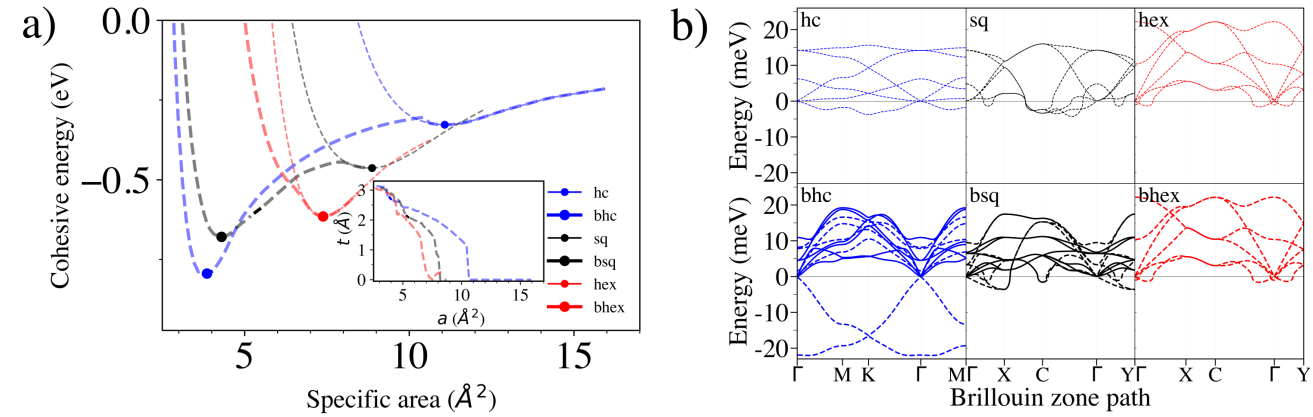

Hg)

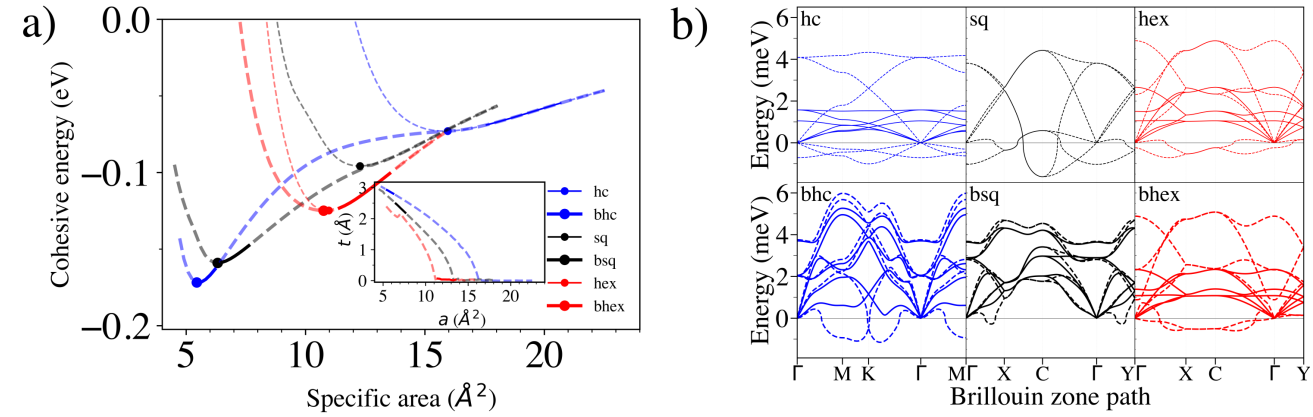

Group 13

Al)

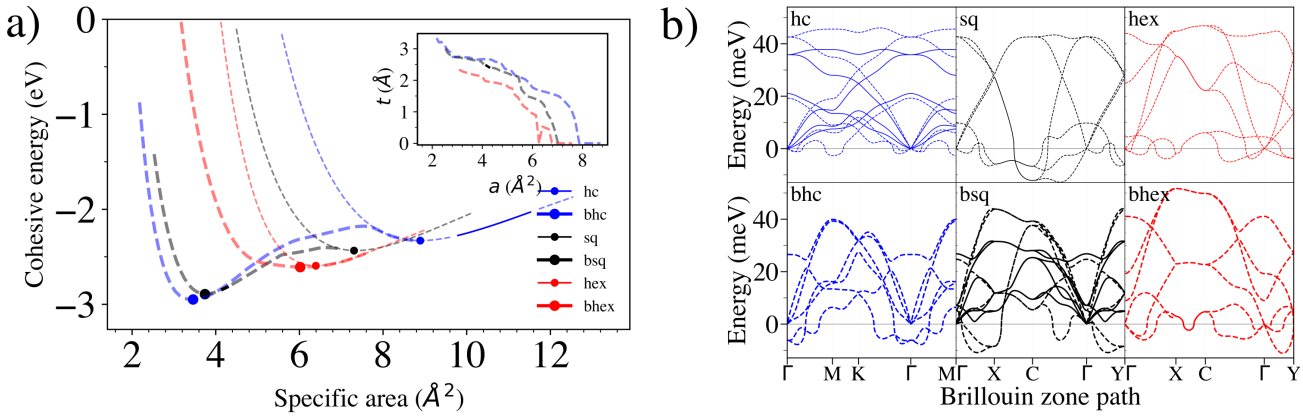

Ga)

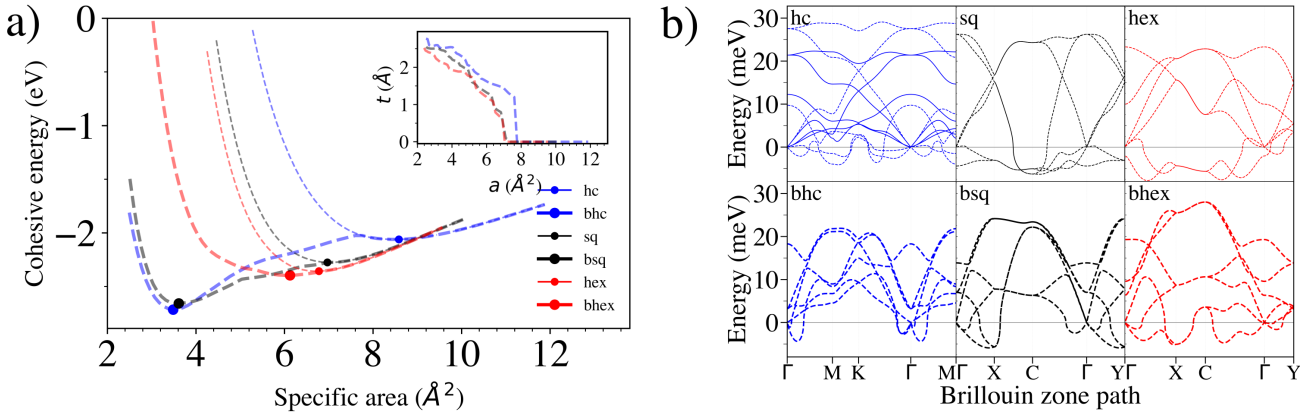

In)

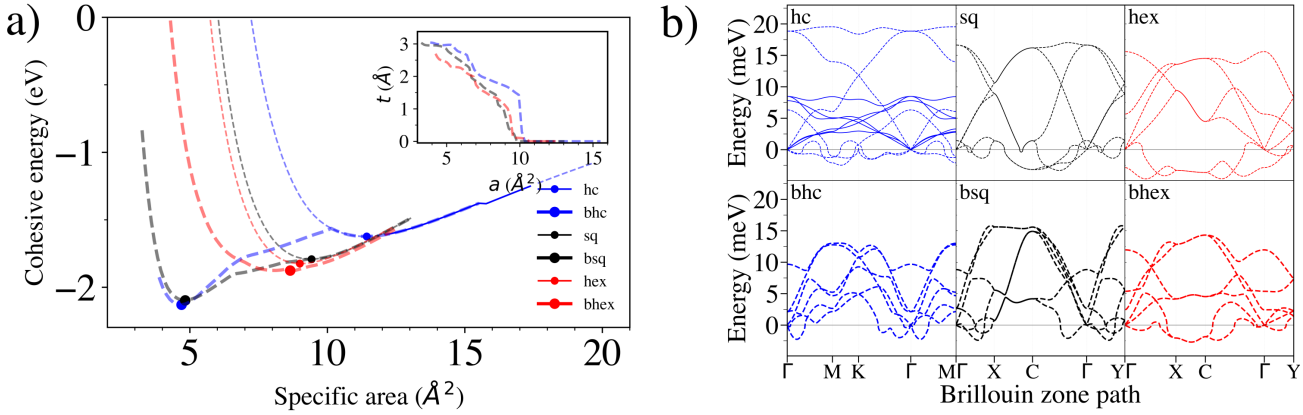

Tl)

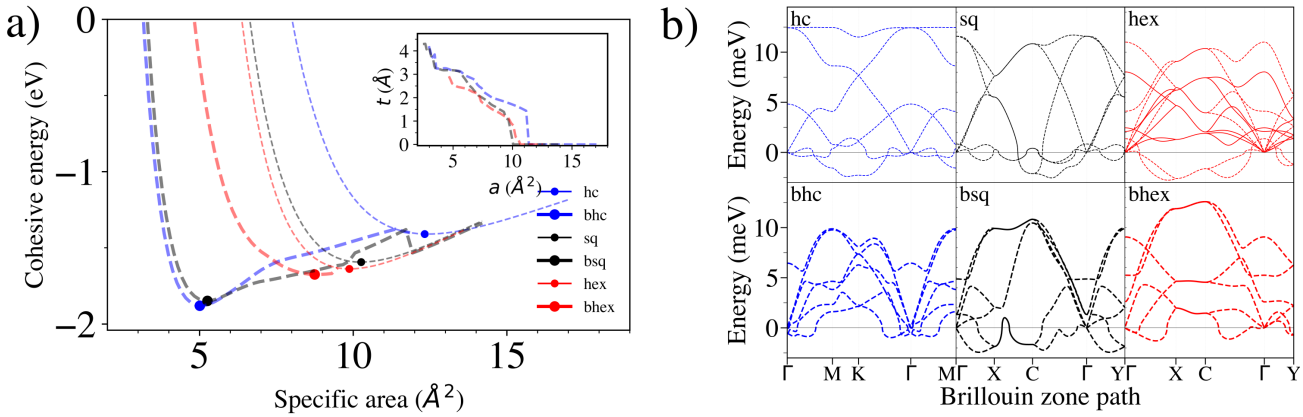

Group 14

Sn)

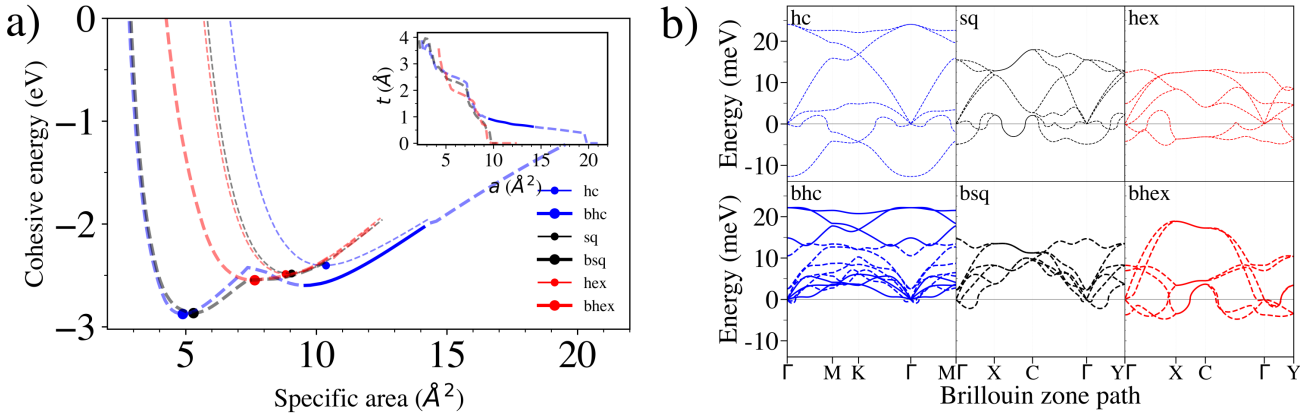

Pb)

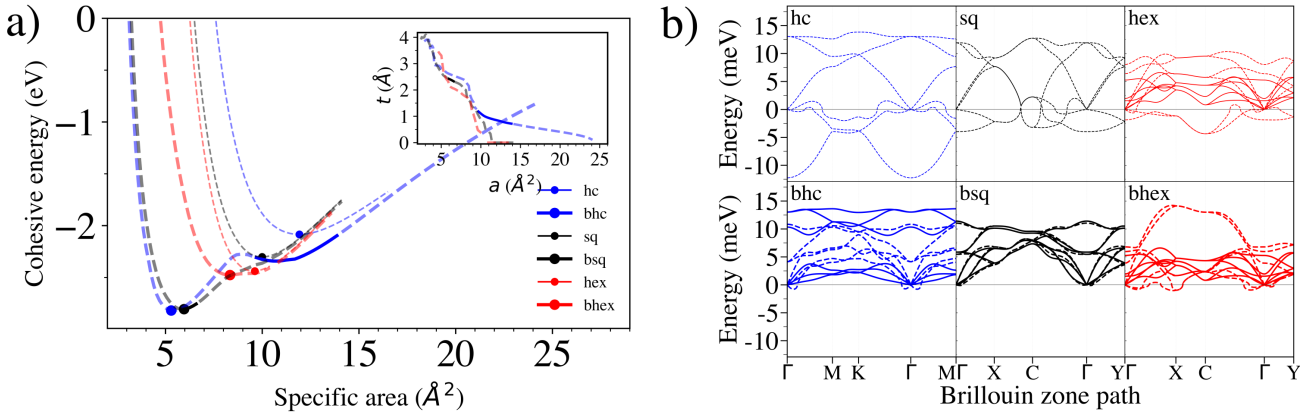

Group 15

Bi)

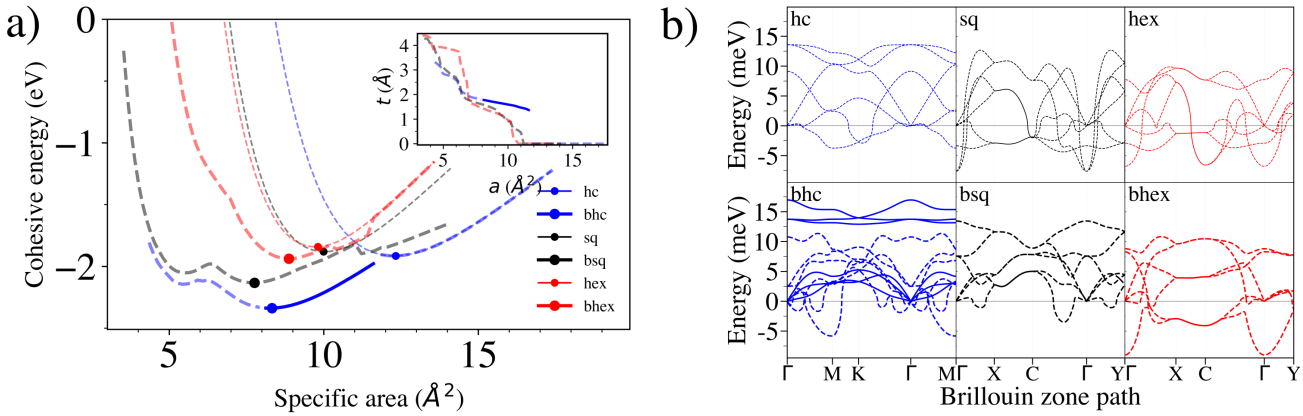

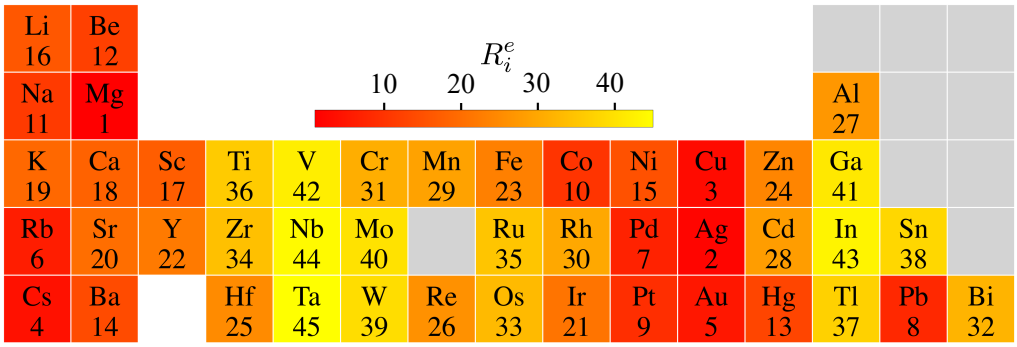

Fig. S5. The rank R_i^e of the dimensionless energetic stability indicator e_i for all metallic elements.

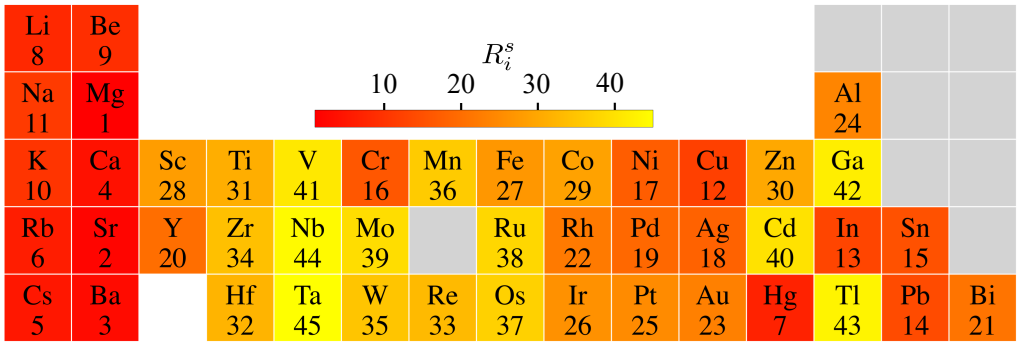

Fig. S6. The rank R_i^s of the dimensionless 2D dynamical stability indicator s_i for all metallic elements.

TABLE I. Cohesive energies E_{coh} (eV), equilibrium areas per atom a (Å^2), and bulk moduli K (GPa-nm) for each lattice.

	bhc			hc			bsq			sq			bhex			hex		
Elements	E_{coh}	a	K	E_{coh}	a	K	E_{coh}	a	K	E_{coh}	a	K	E_{coh}	a	K^*	E_{coh}	a	K^*
Bi	−2.34	8.31	14.10	−1.92	12.36	22.02	−2.13	7.79	18.57	−1.88	10.10	28.47	−1.94	8.96	24.04	−1.84	9.80	29.08
Pb	−2.82	5.48	30.02	−2.09	11.99	14.71	−2.81	5.96	23.29	−2.30	10.07	23.51	−2.48	8.56	13.99	−2.44	9.65	25.53
Sn	−2.88	4.98	32.49	−2.40	10.38	20.05	−2.87	5.32	22.61	−2.48	9.07	24.20	−2.55	7.71	13.51	−2.49	8.94	27.80
Tl	−1.88	5.15	29.89	−1.41	12.53	10.29	−1.85	5.35	25.04	−1.59	10.34	13.10	−1.68	8.72	16.70	−1.64	9.97	13.25
In	−2.13	4.74	33.58	−1.62	11.48	10.85	−2.10	4.91	25.92	−1.79	9.48	15.55	−1.88	8.24	5.74	−1.83	9.11	16.47
Ga	−2.72	3.56	56.10	−2.06	8.54	14.86	−2.66	3.70	37.39	−2.28	7.08	25.60	−2.39	6.13	13.80	−2.36	6.77	25.40
Al	−2.95	3.52	44.62	−2.33	8.96	24.42	−2.89	3.83	56.33	−2.43	7.40	27.68	−2.61	6.07	11.77	−2.59	6.48	33.77
Hg	−0.17	5.67	5.41	−0.07	16.03	0.96	−0.16	6.48	3.05	−0.10	12.42	1.81	−0.12	10.77	1.50	−0.12	11.06	2.72
Cd	−0.80	3.92	38.29	−0.33	11.15	7.62	−0.68	4.38	26.39	−0.46	8.82	9.29	−0.61	7.47	24.93	−0.62	7.49	29.03
Zn	−1.02	3.00	64.20	−0.53	8.57	10.62	−0.84	3.34	37.30	−0.68	6.57	14.15	−0.80	5.78	41.76	−0.91	5.78	41.35
Au	−3.80	3.43	135.34	−2.75	8.57	44.15	−3.62	3.85	112.54	−3.32	7.08	72.87	−3.66	6.57	78.07	−3.66	6.57	81.25
Ag	−2.17	3.68	63.46	−1.44	9.63	16.05	−2.07	4.06	65.03	−1.78	7.51	29.91	−1.99	6.91	33.75	−1.99	6.93	37.61
Cu	−3.04	2.77	77.57	−1.96	6.99	26.93	−2.90	3.05	53.82	−2.41	5.58	47.23	−2.72	5.14	44.90	−2.72	5.17	53.08
Pt	−5.72	3.21	189.61	−4.06	7.90	66.99	−5.44	3.54	112.17	−4.67	6.47	101.59	−5.22	5.95	109.17	−5.21	5.98	129.83
Pd	−3.72	3.22	122.27	−2.10	8.13	41.45	−3.51	3.56	71.85	−2.64	6.54	64.23	−3.04	5.74	48.92	−2.98	6.09	81.54
Ni	−4.77	2.58	117.53	−3.14	6.14	42.98	−4.52	2.85	69.40	−3.67	5.11	64.90	−4.08	4.63	45.56	−3.97	4.76	79.22
Ir	−6.64	3.15	203.99	−5.16	7.38	99.20	−6.22	3.58	104.49	−5.41	6.15	122.78	−6.08	5.52	105.17	−5.83	5.81	144.97
Rh	−5.22	3.11	158.26	−3.66	7.29	67.11	−4.91	3.50	77.91	−4.03	6.07	79.52	−4.44	5.33	64.89	−4.20	5.80	92.21
Co	−4.72	2.64	105.91	−3.13	6.19	41.30	−4.44	2.94	53.56	−3.67	5.12	61.49	−3.99	4.69	32.35	−3.96	4.85	76.58
Os	−7.55	3.17	188.53	−5.47	7.24	104.61	−6.90	3.71	76.96	−5.84	5.99	135.07	−6.49	5.45	106.67	−6.18	5.75	153.95
Ru	−6.09	3.14	132.09	−4.32	7.00	79.38	−5.65	3.58	54.85	−4.74	5.83	108.89	−5.02	5.31	81.41	−4.72	5.68	112.38
Fe	−4.42	2.52	136.38	−2.65	5.43	69.39	−4.47	2.86	88.15	−3.13	4.60	99.87	−3.81	4.63	18.75	−3.80	5.05	59.51
Re	−8.33	3.19	212.40	−5.87	7.16	99.71	−7.67	4.26	73.42	−6.43	5.93	149.09	−6.99	5.14	118.27	−6.70	5.70	175.12
Mn	−2.71	2.63	112.71	−1.19	9.38	11.41	−2.37	3.42	56.56	−1.64	4.65	99.89	−1.88	6.05	12.10	−1.66	4.64	104.72
W	−7.31	3.37	100.25	−4.63	7.53	86.38	−6.94	3.47	171.28	−5.41	6.33	120.87	−6.14	5.31	90.03	−5.85	6.12	132.38
Mo	−4.91	3.23	142.92	−3.14	7.16	75.04	−4.81	3.35	130.67	−3.65	6.11	94.81	−4.11	5.08	74.39	−3.78	5.94	100.58
Cr	−2.75	2.63	36.71	−0.88	5.70	55.65	−2.78	2.67	131.21	−1.64	4.90	96.58	−2.00	4.02	58.30	−1.68	4.84	98.21
Ta	−7.10	3.49	140.74	−4.23	8.39	44.53	−7.07	3.72	98.27	−5.37	6.74	74.52	−6.12	5.57	37.99	−5.84	6.48	91.06
Nb	−5.83	3.47	119.28	−3.49	8.05	30.95	−5.91	3.65	101.47	−4.52	6.70	69.33	−5.15	5.15	53.70	−4.82	6.44	76.37
V	−4.59	2.83	109.50	−2.27	6.32	29.31	−4.72	2.92	93.56	−3.38	5.28	66.83	−3.98	3.85	54.72	−3.53	5.19	65.99
Hf	−5.67	4.28	54.98	−2.86	10.06	25.54	−5.66	4.56	43.85	−4.06	7.65	50.99	−4.62	6.39	26.62	−4.40	7.39	52.45
Zr	−5.63	4.45	33.27	−3.19	10.28	15.44	−5.68	4.63	41.67	−4.31	7.99	42.37	−4.78	6.11	21.38	−4.62	7.61	39.88
Ti	−4.86	3.74	41.87	−2.38	8.10	18.18	−4.93	3.92	39.03	−3.60	6.48	42.90	−4.08	4.54	28.04	−3.78	6.34	40.47
Y	−3.92	5.58	27.09	−1.91	13.93	6.33	−3.82	6.15	19.96	−2.79	10.40	19.19	−3.08	9.70	8.67	−2.99	10.16	20.66
Sc	−3.55	4.79	33.09	−1.50	11.71	8.18	−3.46	5.18	26.94	−2.40	8.65	22.22	−2.65	7.05	12.71	−2.54	8.69	20.85
Ba	−2.02	8.47	9.07	−0.86	24.89	1.87	−1.96	9.12	8.23	−1.36	16.70	5.06	−1.54	16.08	4.69	−1.54	16.32	6.56
Sr	−1.35	7.86	14.80	−0.53	24.32	3.63	−1.24	8.97	10.72	−0.89	23.09	4.77	−0.99	15.74	7.58	−0.99	15.75	7.74
Ca	−1.67	6.75	13.89	−0.65	19.55	2.89	−1.62	7.11	11.20	−1.07	13.17	8.40	−1.23	13.11	8.10	−1.23	13.16	9.41
Mg	−1.39	4.12	38.07	−0.44	12.79	5.54	−1.18	4.73	10.56	−0.65	9.32	12.25	−0.94	8.29	12.47	−0.95	8.39	16.96
Be	−3.18	2.06	77.34	−1.48	6.01	19.10	−2.97	2.26	44.39	−2.35	3.92	49.07	−2.77	3.95	45.98	−2.79	3.91	51.60
Cs	−1.17	12.51	3.25	−0.65	30.16	1.41	−1.11	11.94	4.66	−0.80	23.31	2.98	−0.88	23.52	1.83	−0.88	23.73	2.25
Rb	−1.04	10.55	3.41	−0.64	25.60	1.83	−1.01	10.49	5.21	−0.79	20.39	3.00	−0.85	20.03	2.09	−0.85	20.17	2.77
K	−0.96	8.82	7.67	−0.61	22.86	1.80	−0.90	9.14	5.56	−0.73	17.11	3.68	−0.82	16.89	3.38	−0.82	16.97	3.90
Na	−1.02	5.88	7.68	−0.67	14.44	2.23	−0.98	6.12	5.61	−0.84	11.31	4.63	−0.91	11.23	4.77	−0.91	11.23	4.77
Li	−1.46	4.24	10.57	−0.85	9.74	2.42	−1.44	4.39	8.69	−1.15	8.40	5.85	−1.21	8.28	4.30	−1.21	8.38	5.93

*Assuming elastic constants $C_{11} \approx C_{22}$ for hexagonal systems (using rectangular computational unit cell).

[1] S. Smidstrup, T. Markussen, P. Vancraeyveld, J. Wellendorff, J. Schneider, T. Gunst, B. Verstichel, D. Stradi, P. A. Khomyakov, U. G. Vej-Hansen, M.-E. Lee, S. T. Chill, F. Rasmussen, G. Penazzi, F. Corsetti, A. Ojanperä, K. Jensen, M. L. N. Palsgaard, U. Martinez, A. Blom, M. Brandbyge, and K. Stokbro, Journal of Physics: Condensed Matter **32**, 015901 (2019).

[2] J. P. Perdew, K. Burke, and M. Ernzerhof, Physical Review Letter **77**, 3865 (1996).

[3] M. van Setten, M. Giantomassi, E. Bousquet, M. Verstraete, D. Hamann, X. Gonze, and G.-M. Rignanese, Computer Physics Communications **226**, 39 (2018).

[4] K. R. Abidi and P. Koskinen, Phys. Rev. Mater. **6**, 124004 (2022).

[5] H. J. Monkhorst and J. D. Pack, Physical Review B **13**, 5188 (1976).

[6] D. C. Liu and J. Nocedal, Mathematical Programming **45**, 503 (1989).

[7] K. R. Abidi and P. Koskinen, Journal of Physics: Conference Series **2518**, 012006 (2023).

[8] I. Pallikara, P. Kayastha, J. M. Skelton, and L. D. Whalley, Electronic Structure **4**, 033002 (2022).

[9] S. Radescu, D. Machon, and P. Mélinon, Phys. Rev. Mater. **3**, 074002 (2019).

[10] N. Goga, A. J. Rzepiela, A. H. de Vries, S. J. Marrink, and H. J. C. Berendsen, Journal of Chemical Theory and Computation **8**, 3637 (2012).

[11] H. W. Sheng, M. J. Kramer, A. Cadien, T. Fujita, and M. W. Chen, Phys. Rev. B **83**, 134118 (2011).